Titanium Anodization in *Psidium Guajava*

Anodização de Titânio em *Psidium Guajava*

Anodización de Titanio en *Psidium Guajava*

David de Oliveira Cerveira
ORCID: https://orcid.org/0000-0002-6814-345X
Universidade Feevale, Brazil
E-mail: davidps.oc@hotmail.com
Sandra Raquel Kunst
ORCID: https://orcid.org/0000-0002-8060-3981
Projeto de Fixação de Recursos Humanos do CNPq, Brazil
E-mail: tessaro.sandra@gmail.com
Luã Tainachi Mueller
ORCID: https://orcid.org/0000-0001-5920-9691
Universidade Feevale, Brazil
E-mail: panzermueller@gmail.com
Fernando Dal Pont Morisso
ORCID: https://orcid.org/0000-0002-9653-9857
Universidade Feevale, Brazil
E-mail: morisso@feevale.br
Ana Luiza Ziulkoski
ORCID: https://orcid.org/0000-0003-0850-4003
Universidade Feevale, Brazil
E-mail: analuiza@feevale.br
Roberto Cauduro
ORCID: https://orcid.org/0000-0001-5222-1241
Universidade Feevale, Brazil
E-mail: htcauduro@gmail.com
Cláudia Trindade Oliveira
ORCID: https://orcid.org/0000-0002-4472-5359
Universidade Feevale, Brazil
E-mail: ctofeevale@gmail.com

Abstract
Psidium guajava, commonly known as 'guava', belongs to the Myrtaceae family and is an alternative to the use of traditional methods of corrosion inhibition. The aim of this study is to anodize titanium in an environmentally friendly *Psidium guajava* electrolyte in order to improve its anti-corrosion performance. For this purpose, samples of CP (commercially pure) titanium grade 2 were anodized in plant extract based on *Psidium guajava*, with transient variations of current density (1 and 0.1 mA/cm²) and time (5, 30 and 60 min). Samples were characterized in terms of morphology by SEM (Scanning Electron Microscopy) analysis. The hydrophobicity of oxides was evaluated by the sessile drop method. Anodized samples were analyzed for colorimetry by the CIE L*a*b* method and the electrolyte based on *Psidium guajava* was analyzed by UV-Vis and cyclic voltammetry, in order to understand the compounds and their behavior in the anodizing process. From the obtained results, the oxides generated through anodization at current density of 0.1 mA/cm² were the ones that presented the best performance. The results obtained at 5 and 30 minutes of anodizing showed very similar results and greater reproducibility compared to the others analyzed, which showed the formation of a barrier-type oxide layer in the samples. In the *Psidium guajava* electrolyte, it was evidenced the presence of phenolic groups in its composition, which is believed to influence the process of formation of the oxide layer in the anodization process.
Keywords: Titanium; Anodizing; Implants; Corrosion; *Psidium guajava*.

Resumo
A *Psidium guajava*, comumente conhecida como 'goiaba', pertence à família das Myrtaceae e é uma alternativa ao uso dos métodos tradicionais de inibição de corrosão. O objetivo deste estudo é anodizar titânio em um eletrólito ambientalmente correto de *Psidium guajava* a fim de melhorar seu desempenho anticorrosivo. Para tanto, amostras de titânio CP (comercialmente puro) grau 2 foram anodizadas em extrato vegetal a base de *Psidium guajava*, com variação dos transientes de densidade de corrente (1 e 0,1 mA/cm²) e tempo (5, 30 e 60 min). As amostras foram caracterizadas quanto à morfologia por análises em MEV (Microscopia Eletrônica de Varredura). A hidrofobicidade dos óxidos foi avaliada pelo método da gota séssil. As amostras anodizadas foram analisadas em relação à colorimetria pelo método CIE L*a*b* e o eletrólito a base de *Psidium guajava* foi analisado por UV-Vis e por

voltametria cíclica, com a finalidade de entender os compostos e seus comportamentos no processo de anodização. Dos resultados obtidos, os óxidos gerados por anodização na densidade de corrente de 0,1 mA/cm² foram os que apresentaram melhor desempenho. Os resultados obtidos em 5 e 30 minutos de anodização apresentaram resultados muito semelhantes e maior reprodutibilidade em comparação aos demais analisados e que evidenciou a formação de camada óxida do tipo barreira nas amostras. No eletrólito de *Psidium guajava*, foi evidenciado a presença de grupos fenólicos em sua composição, o que se acredita que influenciam no processo de formação da camada óxida no processo de anodização.

Palavras-chave: Titânio; Anodização; Implantes; Corrosão; *Psidium guajava*.

Resumen

Psidium guajava, comúnmente conocida como 'guayaba', pertenece a la familia de las mirtáceas y es una alternativa al uso de los métodos tradicionales de inhibición de la corrosión. El objetivo de este estudio es anodizar titanio en un electrolito ecológico de *Psidium guajava* para mejorar su rendimiento anticorrosivo. Para ello, se anodizaron muestras de titanio grado 2 CP (comercialmente puro) en extracto vegetal a base de *Psidium guajava*, con variaciones transitorias de densidad de corriente (1 y 0,1 mA/cm²) y tiempo (5, 30 y 60 min). Las muestras se caracterizaron en términos de morfología por análisis MEB (Microscopía electrónica de barrido). La hidrofobicidad de los óxidos se evaluó por el método de gota sésil. Las muestras anodizadas fueron analizadas por colorimetría por el método CIE L*a*b* y el electrolito a base de *Psidium guajava* fue analizado por UV-Vis y voltamperometría cíclica, con el fin de entender los compuestos y su comportamiento en el proceso de anodizado. De los resultados obtenidos, los óxidos generados por anodizado a una densidad de corriente de 0,1 mA/cm² presentaron el mejor desempeño. Los resultados obtenidos a los 5 y 30 minutos de anodizado mostraron resultados muy similares y mayor reproducibilidad en comparación con los demás analizados, lo que mostró la formación de una capa de óxido de tipo barrera en las muestras. En el electrolito de *Psidium guajava* se evidenció la presencia de grupos fenólicos en su composición, los cuales se cree influyen en el proceso de formación de la capa de óxido en el proceso de anodización.

Palabras clave: Titanio; Anodizado; Implantes; Corrosión; *Psidium guajava*.

1. Introduction

Titanium is a metal that has excellent properties of biocompatibility and resistance to corrosion, which have been propelled its application in several sectors, mainly in the medical field. The use of titanium in prostheses of hip and knee is quite known, as well as its applicability in plaques, screws, and pegs for traumas. However, titanium and its alloys can also enable the development of bioactive implants, external prosthesis, and instrumentation. Some of the advantages of titanium or titanium alloys for biomedical applications are as follows: biocompatibility, since titanium is more resistant to traction than human bones (80-120 Mpa), stainless steel, and other implant materials; high fatigue resistance (50% greater than the merge alloy of Co-Cr); high impact resistance; good corrosion resistance; lower elastic modulus than iron or cobalt alloys, and low density (Ory et al., 2018; Verma et al., 2020; Saurabh et al., 2022).

There is no register of other surgical procedure like osseointegrated implants that has proven such an impact in the life quality of people that for any motive do not have one or more teeth. However, failures and intercurrences in treatments of oral rehabilitation are possible setbacks that represent an increase in therapeutic time, additional costs, discomfort for the patient and constraint for the professional. Studies claim that a significant number of implant failures have been reported recently. The occurrence of failures in osseointegrated implants is not rare, since the rate of failures can vary between 1.5% and 3.5%, which may achieve approximately 10%. The cause of the failures, as well as the mechanisms responsible for defect or loss of implants are multifactorial, as local, systemic, and genetic factors may coexist. Additionally, these factors may be related to the patient and technique applied by the professional, and also to the material used or the correlation of both. In this context, the improvement of superficial and biocompatible characteristics of implants have gained more attention with the aim of reducing even more failure indices of procedures (Alves, 2008; Amorim et al., 2019; Hsueh et al., 2020).

Even considering the resistivity of implantable titanium, this material is susceptible of corrosion when in contact with human body and its biological fluids. In this sense, it is possible to use varied types of superficial treatments with the aim of increasing its oxide layer (TiO_2) (naturally formed when the material comes in contact with the air) for the improvement of anticorrosive capacities of titanium. Titanium in the form of oxide, i.e., the layer of titanium dioxide (TiO_2), is responsible for

intimate adaptation of implants, named as osseointegration or functional ankylosis, that occurs between the mineralized bone and the surface of the implant, reducing or turning inexistent the reaction of tissue with the implant or material used (Galan, 2013; Rahman et al., 2016; Fernandes et al., 2022).

Industrially, anodization has been shown as the easiest process of fabrication of titanium oxides, since it enables the obtention of these oxides in barrier, porous, and sparking forms. During the process of titanium anodization, acid-based electrolytes, mainly sulfuric acid (H_2SO_4) and chloridric acid (HCl), are generally used. However, the discharge of these electrolytes after its use in anodization is done by effluent treatment, since they have physicochemical characteristics that may alter the receptor body (river, lake, etc.) and harm the local ecosystem. In this sense, environmentally correct electrolytes may be an alternative to minimize the harmful effect of the process. Therefore, the *Psidium guajava* extract is a natural compound harmless to the environment, that may be considered as environmentally correct. Since it has no physicochemical characteristics that may interfere in the receptor body, it can be discharged without effluent treatment, which also assists in reducing costs for the industry (Mueller et al., 2019; Indira et al., 2015).

The development of ecologically correct technologies and green strategies have been shown as quite feasible alternatives, as well as the use of plant extracts. In this sense, plant materials seem to be an alternative for the substitution of corrosion inhibitors, such as the synthetic ones, which are expensive and toxic. Plant extracts present several benefits, including less environmental risk, lower cost, widespread availability, and high efficacy of corrosion inhibition. Therefore, the oxidant effect of *Psydium guajava* in anodization are mainly related to its phenolic compounds (Umoren et al., 2019). (Poly)phenolic derivatives that are present in the plant extract probably adsorb over the metallic surface, and in the presence of potential or current, they form phenoxyl radicals and corresponding quinones that will act as oxidants in the anodizing process, being consumed in this process (Naseer et al., 2018). In this sense, the aim of the present study is to anodize titanium in an environmentally correct electrolyte in order to improve its anti-corrosion performance and study the compounds of the plant extract based on *Psidium guajava*.

2. Methodology

A CP titanium milled sheet grade 2 with 1.0 mm thickness was acquired from Titânio Brasil Ltda and used to perform this study. Samples were cut from the sheet in a rectangular shape with a width of 4.5 cm and a length of 5.1 cm (anodized area of 45.9 cm²). CP titanium grade 2 presents chemical specifications required by ASTM F67 for applications in surgical implants, as certified by the supplier. Table 1 details the chemical composition required for classifying the sheet as titanium.

Table 1. Maximum composition allowed for CP titanium grade 2.

Element	Composition (%)
Nitrogen, max	0.03
Carbon, max	0.08
Hydrogen, max	0.015
Iron, max	0.30
Oxygen, max	0.25
Residues, max each	0.1
Residues, total max	0.4
Titanium	Balance amount

Source: (ASTM F67).

2.1 *Psidium guajava* extract

Guava seeds were collected in different days and at different times of the day at temperatures that varied between 20 and 32 ºC. Subsequently, the seeds were washed in running water and the excess of humidity was taken with a cloth. The seeds were left overnight in an opened recipient to initiate the drying process. After drying, the seeds were shredded in a conventional blender and stored in a closed recipient in a heat- and humidity-free environment.

For preparation of the extract, 120 g of the shredded extract was added to a becker containing 3 L of water. A stirrer was used at a rotation of 650 rpm and the mixture was covered and left for 15 minutes when it reached 38 ºC. The mixture passed through sieve to eliminate shreds of seeds before filtering. Then, a vacuum filtration apparatus was used, which was composed of a 1 L Kitasato flask, a Büchner funnel, a vacuum pump, and filter paper. After filtration, the filtered liquid was transferred to 1 L amber recipients and labelled. Afterwards, the recipients were put in a conventional refrigerator for until 48 hours. The measured pH was 5.5.

2.2 Anodization process

Anodizations were performed with the use of a voltage source of 300 V – 500 mA coupled to a computer containing a software for data recording. Anodizations were carried out in galvanostatic mode with current density variations of 1.0 and 0.1 mA/cm², temperature between 7 and 1.4 ºC of the *Psidium guajava* extract (original extract), and pH of 5.5 measured at 5, 30, and 60 minutes. The sample was connected as the anode and titanium was used as the cathode.

The identification of samples, according to these parameters, is described in Table 2. Two samples were evaluated in each anodization condition.

Table 2. Identification of samples.

Nomenclature	Current density (mA/cm²)	Time (min)	Temperature (°C)
Pure; not anodized	--	--	--
TI1-5	1	5	7
TI1-5A	1	5	1.4
TI01-5A	0.1	5	7
TI01-5	0.1	5	1.4
TI01-30	0.1	30	7
TI1-30	1	30	1.4
TI1-30A	1	30	7
TI01-30A	0.1	30	1.4
TI1-1HA	1	60	7
TI01-1H	0.1	60	1.4
TI01-1HA	0.1	60	7
TI1-1H	1	60	1.4

Source: Authors.

2.3 Characterization of the anodized layer surface

Colorimetric studies were performed with the use of a spectrophotometer (CM5 model, Konica Minolta) and a computer for data collection. For results' obtention, samples were analysed by using the sample "Pure; not anodized" as reference, applying the diffused light D65 and using an observation angle of 10º.

For SEM analysis, the SEM equipment used was the JSM-6510LV model of the brand Jeol. Samples were metallized with gold target for electrical conduction and images' obtention. After metallization, samples were analysed in terms of top-

view morphology.

The analysis of contact angle was performed by using an equipment for measuring the contact angle (OCA 15EC model, Labcontrol). A syringe with a needle of 0.4 mm and deionized water were also used to perform the tests, and 8.3 µL were deposited with a flow rate of 2.0 µL s^{-1}. The assay was performed in triplicate and data acquisition was through the SCA20_u software (Dataphysics Instruments).

Tests were performed in a UV-Vis spectrophotometer (Lambda 265 model, PerkinElmer). Samples of *Psidium guajava* extract were used before and after the anodization at 0.1 mA/cm² and at 5 and 30 minutes, which refers to processes that presented better reproducibility results. Samples were diluted in ultrapure water in a dilution ratio of 1:2000. Tests were performed at a wavelength between 200 and 900 nm. The equipment was previously calibrated with ultrapure water.

Aiming to analyze the voltammetric profile and the reproducibility of the Ti/oxide/electrolyte system, cyclic voltammetry measurements were performed in a potentiostat (PGSTAT 302, Autolab), in which the CP titanium grade 2 was used as working electrode, saturated calomel electrode (SCE) was used as reference electrode, and platinum was used as auxiliary electrode. The exposed measurement area of the electrochemical analysis was 45.9 cm² ± 0.2 cm². Before performing the assay, the electrolyte was deranged with nitrogen for 1 hour and the pH was measured, resulting in 5.5. The voltammetry was registered in the range between -1.8 V to 1.8 V, in which the scan rate is 1 mV.s^{-1}, potential step of 50 mV, and amplitude of 2 mV.

3. Results and Discussion

3.1 Analysis of anodization curves

Figure 1 shows transient current density (1 and 0.10 mA/cm²) and transient potential of samples anodized in the electrolyte of *Psidium guajava* extract for 300, 1800, and 3600 seconds. For better visualization of phenomena, graphs were plotted in 3600 seconds of anodization.

In Figure 1, a distinct behavior of samples was observed as a function of current density. According to the potential transients, samples presented a constant anodization rate ($\partial V/\partial t$) until the initial seconds of anodization, regardless of the time (5, 30 or 60 minutes). According to Sul, 2001, the formed oxide is in the type of barrier during the initial stages of anodization. The slope of the potential curve, named as anodization rate, is related to the growth of the oxide. It is known that the anodization rate of titanium, which represents the thickening of the film, is normally 1 to 3 nm/V. However, the highest anodization rate was observed in samples anodized at 1 mA/cm² (0.25 V/s) compared to those anodized at 0.1 mA/cm² (0.02 V/s). It was observed that measured values of $\partial V/\partial t$ were proportional to the applied current density, decreasing an order of magnitude. A study performed by Quintero et al., 2014 showed a strong dependence of the current density on the thickness and formation kinetics of films anodized in CP titanium grade 2, using an electrolyte of 1.5 M H_2SO_4/0.3 M H_3PO_4. The authors compared oxides grown by galvanostatic anodization at 15 mA/cm^{-2}, 35 mA/cm^{-2}, and 55 mA/cm^{-2}, identifying that a so-called "duplex" system is formed in all samples, which means that the oxide layer adjacent to the metal is a thin and compact barrier-type layer, and on the top of it, another thicker and porous-type film layer grows. The porous anodic film obtained by the authors at 15 mA/cm² had an average thickness of 4.70 ± 0.15 µm and the inner layer had an average thickness of 0.19 ± 0.04 µm. At 35 mA/cm², the average thickness of the porous layer was 10.61 ± 0.50 µm and that of the inner layer was 0.51 ± 0.08 µm. Regarding the film obtained at 55 mA/cm², the average thickness of the porous layer was 14.68 ± 0.60 µm and of the inner layer was 0.88 ± 0.10 µm.

Figure 1. Transients of titanium anodized in *Psidium guajava* extract. Current density transients and potential transients of titanium anodized in *Psidium guajava* extract at current densities of 1 (mA/cm²) and 0.1 (mA/cm²) and at anodization time of 5 minutes (300 seconds), 30 minutes (1800 seconds) and 60 minutes (3600 seconds).
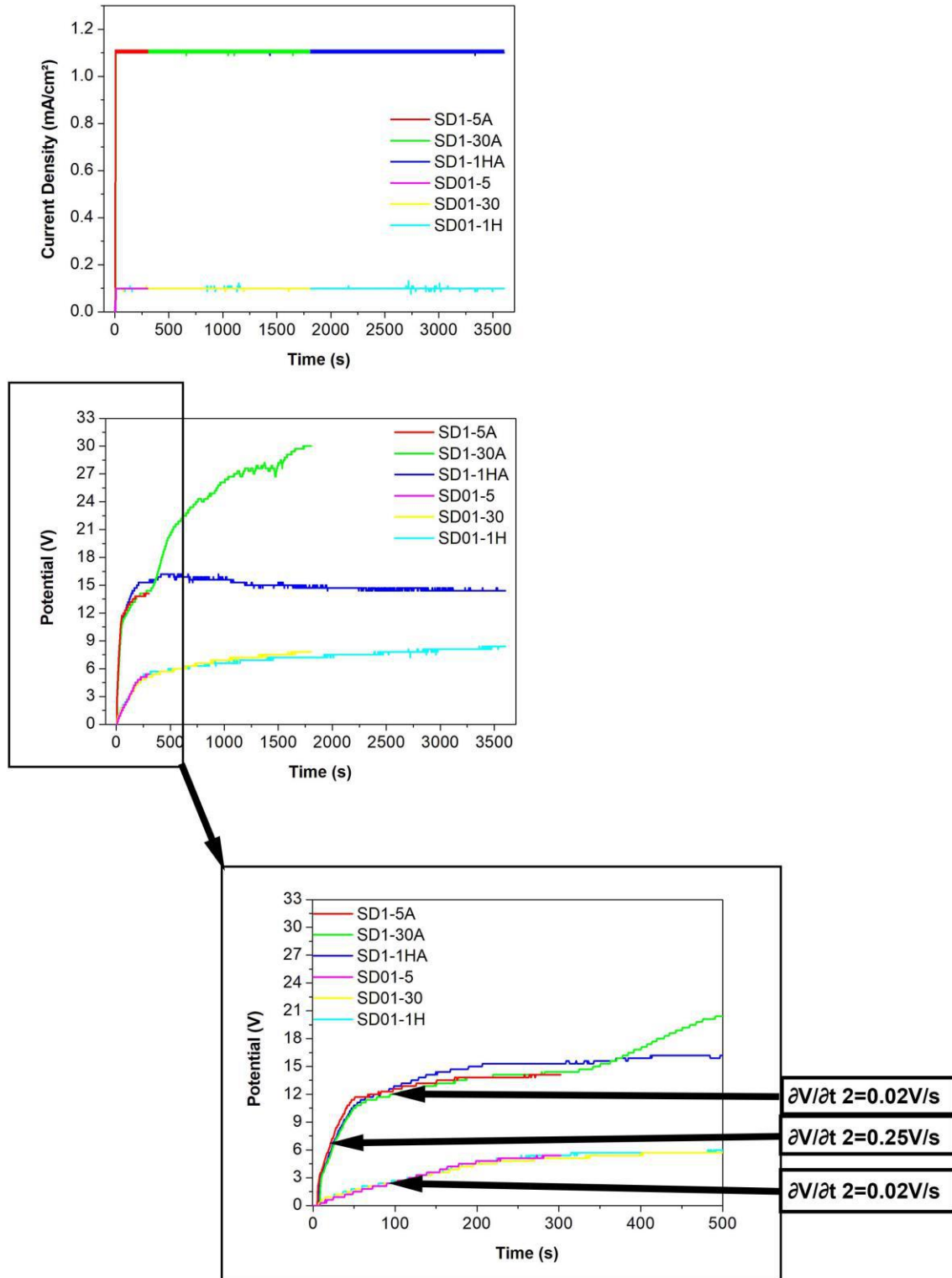

Source: Authors.

Samples anodized at 1 mA/cm² showed a second growth rate after 40 seconds of anodization, $\partial V/\partial t_2 = 0.02$ V/S,

which corresponds to the $\partial V/\partial t$ observed in samples anodized at 0.1 mA/cm². However, the current density remains constant for samples anodized at 1 mA/cm², despite the growth rate decreasing after 12 V. According to Nakajima et al., 2009 and Kociubczyk et al., 2015, this variation of $\partial V/\partial t$ in valve metals may be due to the occurrence of sparking (phenomenon of light emission that is related to the rupture of the anodic oxide film due to electrical characteristics, such as critical values of voltage or current), accompanied by dielectric breakdown. Sparking is characterized by the occurrence of sparking in the sample, causing the crystallization of the oxide film. However, no characteristic was observed that could identify sparking during anodizations, and the literature shows that the sparking potential for titanium anodized samples occurs at potentials above 100 V (Kuromoto et al., 2007; Nakajima et al., 2007; Nakajima et al. al., 2009; Liu et al., 2014).

Conversely, the second slope of the anodization transient may be due to the consumption of electrolyte species, since the electrolyte is composed of phenolic species that are basically formed of C, H, and O. It was observed that the potential increases up to 30 V (Ti1-30A) or remains stable at 15 V (Ti1-1HA) after 200 seconds during anodization at higher current density (1 mA/cm²), indicating that there is no reproducibility during the process. Regarding the samples anodized at lower current density (0.1 mA/cm²), a similar behavior is observed at all anodization times. It is generally believed that the electrochemical behavior of the growth of titanium anodic oxides is due to the electrochemical dynamics between formation rates and dissolution rates of the film. These, in turn, depend on the nature of the electrolyte (Young et al., 1971; Sul et al., 2001; Fuhr et al., 2020).

The species found in greater quantity in the electrolyte of *Psidium guajava* are phenolic compounds based on C, H, and O. The anodization of valve metals occurs through the combination of OH species of the electrolyte that come into contact with the metal, giving rise to the formation of the oxide. Electrochemical corrosion of metals and alloys are represented by the schematic current-potential curve presented in Figure 2. This curve is also called as potentiokinetic curve or anodic polarization curve. Three regions can be distinguished on this curve. The first region corresponds to the active state of the metal, in which the anodic dissolution occurs according to the overall reaction presented in Equation 1.

$$M \rightarrow M^{n+} + ne^- \qquad (1)$$
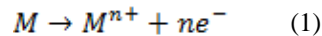
In the reaction (1), the "M" refers to the surface metal atoms that switch to the aqueous solution in the form of cations, which are consequently hydrolyzed. A number (n) of electrons are exchanged in this electrochemical reaction. In this region (the rising part of the peak), the current density is an exponential function according to classical electrochemical kinetics. The second region, as shown in Figure 2 for passive metals, corresponds to the passive state of the metal. It starts with a transition from the active state to the passive state, which is responsible for the appearance of the peak in the current-potential curve. Above the critical passivation potential (the maximum of the active peak), an oxide (or oxyhydroxide) film grows on the surface and the dissolution current drops to a value that is, typically, several orders of magnitude lower than the anodic dissolution current in the maximum of the active peak. The surface of the metal is considered to be passivated, or the metal is considered to be in the passive state. The anodic oxidation reaction is shown in Equation 2.

$$nM + mH_2O \rightarrow M_nO_m + 2mH^+ + 2me^- \qquad (2)$$
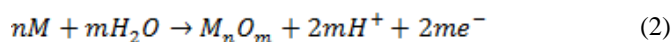
The passive region usually extends to a significant range of potentials (a few hundred mV). The third region on the polarization curve is the transpassive region, in which the current density starts to increase as long as the potential further increases. In this region, the increase of material dissolution occurs under conditions in which electrochemical polishing can be performed. In passive films with appropriate semiconductor properties, oxygen evolution can occur as shown in Equation 3.

$$2H_2O \rightarrow O_2 + 4H^+ + 4e^- \qquad (3)$$
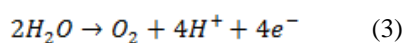
In the case of Al and other metals, such as Ta, Zr, Nb, and Ti (generally called valve metals), the surface oxide films are insulating and become thicker with increasing potential. In this situation, oxygen evolution does not occur, and the passive region extends to a few Volts before dielectric breakdown of the oxide film occurs. When impurities or aggressive anions (as

for example, Cl⁻) are present in the aqueous solution, an increase in the current density can be observed at a potential located in the passive region, i.e., below the transpassive potential. This effect is caused by local breakage of the passive film and by localized dissolution. The early stages of this important phenomenon are generally called as pitting corrosion (Marcus et al., 2000).

It is important to notice that the anodic (oxidative) reactions presented in Figure 1 are half-reactions, which means that a cathodic (reductive) reaction must occur simultaneously at the surface to satisfy zero net current conditions.

Figure 2. Anodic polarization curve (current density versus potential) of a metallic material demonstrating active, passive and transpassive regions of anodic dissolution.
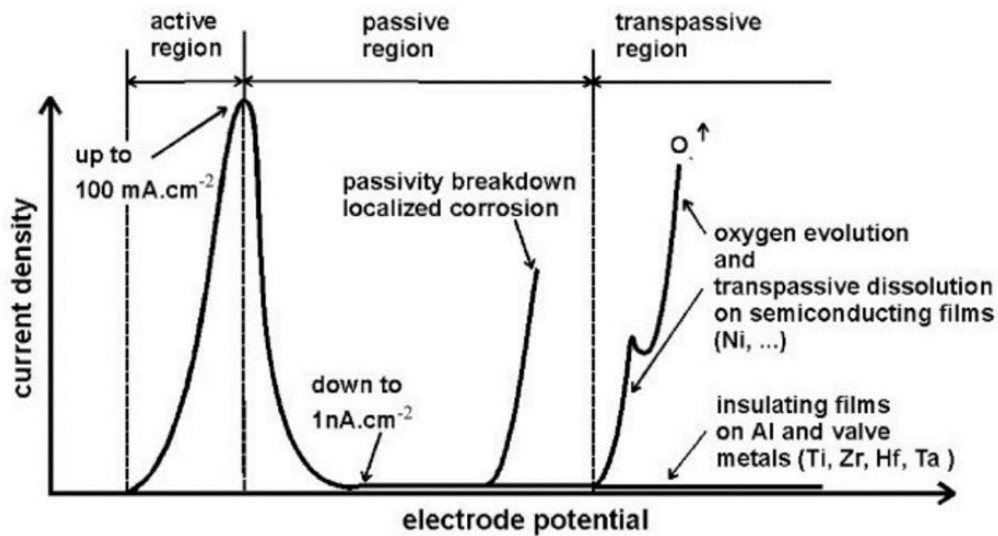
Source: Adapted (Marcus et al., 2000).

The cathodic reaction can be the reduction of protons from the solution (Equation 4) or the reduction of dissolved oxygen in the aqueous solution (Equation 5).

$$H^+ + e^- \to \tfrac{1}{2} H_2 \qquad (4)$$

$$\tfrac{1}{2} O_2 + 2H^+ + 2e^- \to H_2O \qquad (5)$$
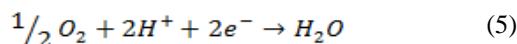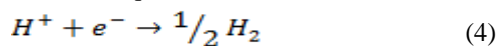
In practical situations, both anodic and cathodic reactions take place on the surface of the material. This is an important point as it can be immediately understood that, although the fundamental corrosion reaction is the anodic dissolution, it necessarily involves a cathodic reaction, which can be used as means of controlling the corrosion rate in some cases (Marcus et al., 2000).

Mechanisms based on classical models and on recent data concerning stages of passive film formation are shown in Figure 3. Point 1 shows where dissociative adsorption of H_2O or adsorption of OH groups occur, which result in surface hydroxylation. Additionally, it is shown that the film growth can occur in two ways (a or b), depending on the following factors: nature of the base metal, relative stability of oxides and hydroxides, pH of the electrolyte, passivation potential, and temperature.

The formation method "a" of Figure 3 initiates with the recombination of adjacent OH- group (dehydration) or deprotonation, causing the formation of oxide islands with thickness of monolayers (item 2a). Subsequently, superficial hydroxylation and lateral growth of oxide islands occur with the formation of a complete oxide monolayer with surface hydroxyl groups (item 3a). Concluding the process, the growth of an oxide that still presents surface hydroxylation would occur perpendicularly to the surface (item 4).

The formation method "b" of Figure 3 starts with the growth of a hydroxide or oxyhydroxide layer perpendicular to the surface, covering the metal completely (item 2b). Afterwards, dehydration/deprotonation and formation of oxide islands occur in the inner part of the passive film (item 3b), as well as lateral growth of islands followed by the formation of a complete inner oxide layer under an outer layer of hydroxide or oxyhydroxide (item 4). This process of advancing the reaction can cause the almost complete dehydration of the passive film with only one monolayer of hydroxide or oxyhydroxide remaining on the surface (Marcus et al., 2000).

Figure 3. Mechanisms of initial formation of passive films.
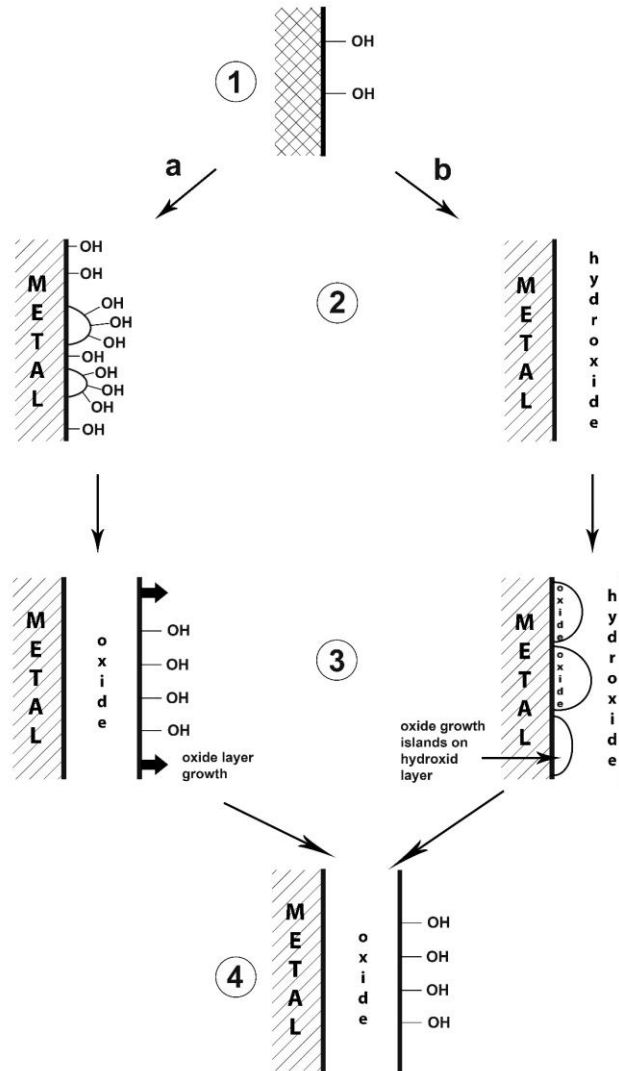
Source: Adapted (Marcus et al., 2000).

Studies on the aluminum anodization process (Lee et al., 2008) demonstrate that the reaction involved in the production of the anodic oxide layer is exothermic, whereas its dissolution is endothermic. However, the main contribution to heat generation in aluminum anodization is related to the current flow through the barrier layer that is part of the oxide. The proportion of the amount of heat in joules is proportional to the square of the current density. The anodization process called hard anodization is an industrial anodization process carried out at relatively low levels of temperature and at high current density (above 50 mA/cm²), using H_2SO_4 as the electrolyte. This process has been routinely used for several industrial

applications that, along with the growth rate of the anodic layer (50-100 µm/h), result in high technical quality. However, the pores of the anodic layer are less organized and more prone to irregularities. In this type of process, there is a large h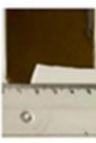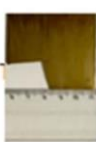eat evolution due to the high anodic current associated with high electric field in the barrier layer. Excessive heat not only causes irregular growth in the anodic layer but also promotes unwanted dissolution of the oxide film generated in the acid solution.

Therefore, it is possible to observe that samples anodized at a higher current density, 1 mA/cm² (TI1-5A, TI1-30A and TI1-1HA), did not show reproducibility. The longer the anodizing time, the greater the difference in relation to the others due to the consumption of electrolyte species over time. In the present study, the second slope of the curve of 1 mA/cm² samples and the lack of reproducibility of the anodization process may be associated with the rapid consumption of electrolyte species. In this case, the reaction rate would be controlled by the transport of species along the electrolyte.

3.2 Visual analysis of color of anodized samples

Figure 4 shows photographs of titanium samples, after anodization in *Psidium guajava* extract, in relation to the time and the current density applied in the process. It is visually observed that there was a difference in the color of samples according to current density and anodizing time.

Figure 4. Photographs of samples anodized in *Psidium guajava* extract in relation to time and applied current density.

Source: Authors.

The fact that samples showed varied colors of oxide layers after the anodization process may be due to stoichiometric defects in the film composition or interference phenomena that cause the coloring. The color change observed in samples presented in Figure 4 indicates the formation of an oxide film on the surface of the substrate resulting from the anodization process. According to Sul, 2001, the color change is directly related to the variation in the developed potential and to the thickness of the formed film.

During the anodization process, each applied potential will result in a characteristic color, which may change

according to the anodization time, electrolyte composition and current density applied. This explains the fact that samples anodized at 0.1 mA/cm² (Figure 3, item g to l) showed little color difference at the same anodization time. In contrast, samples anodized at 1 mA/cm² (Figure 3, item a to f) did not show reproducibility, and the longer the time, the greater the difference in color. This is in line with anodization curves and probably occurs because interferences of the *Psidium guajava* extract compounds generate difference growth constants (nm/V) influenced by the anodization time (nm/s), which consequently cause an alteration in the stoichiometry of the anodic oxide. This means that the longer the anodization time, the greater the difference in relation to the others, which is also due to the consumption of electrolyte species over time.

3.3 Colorimetry

Colorimetry measurements were obtained according to the CIE L*a*b* color space, which provides a more accurate color differentiation with respect to human perception. Even though a varied spectrum of colors has been identified in samples due to the anodization process, it is not possible to verify whether there was reproducibility in the coloration only by visual inspection. Thus, colorimetric measurements were performed for all samples presented in Figure 4 for better identification of colors, and the corresponding values of chromatic coordinates are demonstrated in Table 3.

Table 3. Color coordinates (L*a*b*) for oxides formed during the titanium anodization in *Psidium guajava* extract, in relation to current density and time.

Sample name	Current density (mA/cm²)	Anodization time	L*	a*	b*
Pure-Ti			70.949	0.6227	2.6822
TI01-5		5	66.2742	1.0829	9.7195
TI01-5A		5	66.0273	1.0356	8.945
TI01-30	0.1	30	59.7651	2.2582	20.4418
TI01-30A		30	59.6113	2.1998	19.8043
TI01-1H		60	49.4419	6.4699	31.5151
TI01-1HA		60	52.5706	5.2572	30.6811
TI1-5		5	41.2913	8.5142	1.7083
TI1-5A		5	41.705	7.6464	0.7577
TI1-30	1	30	52.5186	-3.4271	-12.3207
TI1-30A		30	62.248	-8.4459	-6.3499
TI1-1H		60	53.4538	13.848	21.9513
TI1-1HA		60	41.4666	4.5762	-21.9929

Source: Authors.

In Table 3, it was observed that L* values of samples anodized at 0.1 mA/cm² decreased with increasing anodization time, which indicates darker colors. This is in accordance with anodization graphs and with images of samples presented in Figure 4. Values of the a* and b* axes were positive for all samples, and b* values always greater than a* values, which means that the b* value is predominant. This indicates yellow/brown tones, demonstrating the reproducibility of the anodization process at 0.1 mA/cm². As can be seen in Table 3, there was a significant difference in values associated with the chromatic coordinates presented for samples anodized at 1 mA/cm². It is possible to observe that there was no reproducibility in the colorimetric measurements, which agrees with photographs presented in Figure 4 and the anodization graphs (Figure 1). Regarding the luminosity (L *), samples anodized at 1 mA/cm² showed very different values even for the same anodization time, indicating different shades.

Values of the a* and b* axes indicated different colors for all anodized samples, with variations from yellow (Sample

TI1-1H, b=21.9513) to blue (Sample TI1-1HA, b=-21.9929). Unlike samples anodized at current density of 0.1 mA/cm², samples anodized at 1 mA/cm² showed significantly greater differences in values for the same anodization time, characterizing the proof of the visual difference shown in Figure 4 and reinforcing the lack of reproducibility of the anodization process in these samples. Furthermore, the obtained chromatic values correlate well with the visually observed colors. Thus, it is clear that chromatic coordinates are really useful to control the progress of titanium anodization, especially when color differentiation is an important feature for oxide coatings (Zaniolo et al., 2018).

According to the study performed by Sul, 2001, colors of the anodic oxide titanium expressed by the hue (a* value) were dominated by the thickness of the anodic oxide within the range in which the anodizing forming voltage increased almost linearly with anodization time. However, it was observed that not only the value of a*, but also values of L* and b* showed considerable differences according to the electrolytes used, although the anodic oxide thickness and the formation voltage were the same. The authors also verified that, although the anodic oxide films are prepared at the same formation voltage and in the same investigated electrolyte, the corresponding colors of the titanium oxide vary (Sul, 2001). In the case of the present study, the current density directly influences the anodization of titanium, since it accelerates the consumption of electrolyte species, impacting the observed coloration and the reproducibility of the process.

3.4 SEM analysis of non-anodized/anodized samples in Psidium guajava extract

Aiming to analyze the morphology of samples before and after the anodization process, SEM micrographs were obtained of the top view of non-anodized (pure) samples and samples anodized in the electrolyte of *Psidium guajava* extract for 5, 30 and 60 minutes at 0.1 mA/cm², at 1000x and 15000x magnification. Due to the non-reproducibility of samples anodized at a current density of 1 mA/cm² confirmed in anodization curves (Figure 1), visible color (Figure 4), and colorimetry (Table 3), the morphological analysis was performed only on samples anodized at 0.1 mA/cm². The anodization process of samples was performed in duplicate on this study. Thus, two sets of images of SEM micrographs were obtained for each time (5, 30, and 60 minutes) of the current density 0.1 mA/cm².

Figure 5 shows the top-view SEM micrographs of pure samples (not anodized in the electrolyte of *Psidium guajava* extract) at 1000 and 15000x magnification:

In the micrographs, it is possible to observe the existence of irregularities on the surface of the pure titanium sample, which may be associated with the manufacturing process. It is known that the formation of the passive layer of titanium dioxide (TiO_2) occurs naturally on its surface when in contact with oxygen at room temperature. However, this air-formed layer has low surface hardness and low wear resistance. Therefore, this layer is not sufficiently effective to protect CP titanium in some aggressive environments due to its thin thickness (Chen et al., 2013; Catauro et al., 2014).

Figure 5. Top-view SEM micrographs of titanium samples under non-anodized conditions. A) 1000x magnification and B) 15000x magnification.
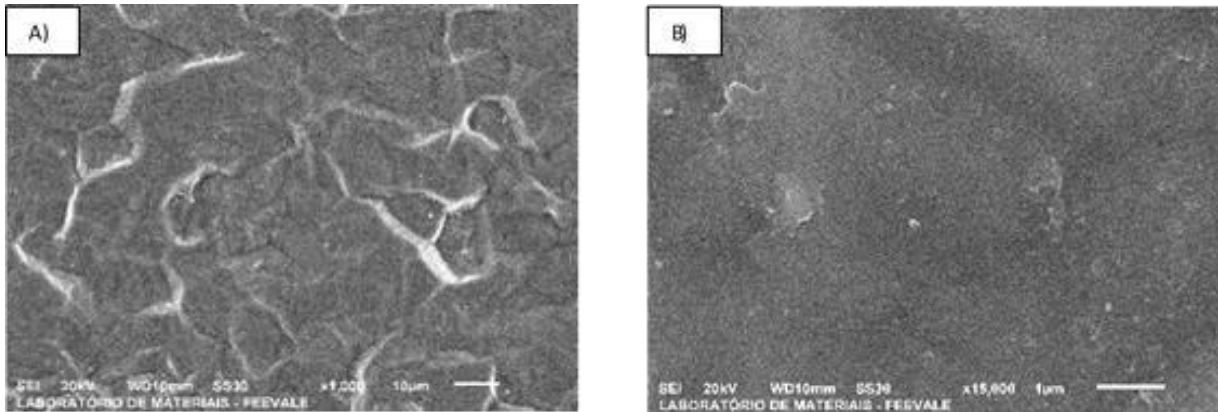
Source: Authors.

Figure 6 shows the top-view SEM micrographs of two samples anodized in the electrolyte of *Psidium guajava* extract for 5 minutes at 0.1 mA/cm², at 1000x and 15000x magnification.

Figure 6. Top-view SEM micrographs of titanium samples anodized in *Psidium guajava* extract for 5 minutes at 0.1 mA/cm². Sample 1 A) 1000x magnification and B) 15000x magnification. Sample 2 C) 1000x magnification and D) 15000x magnification.
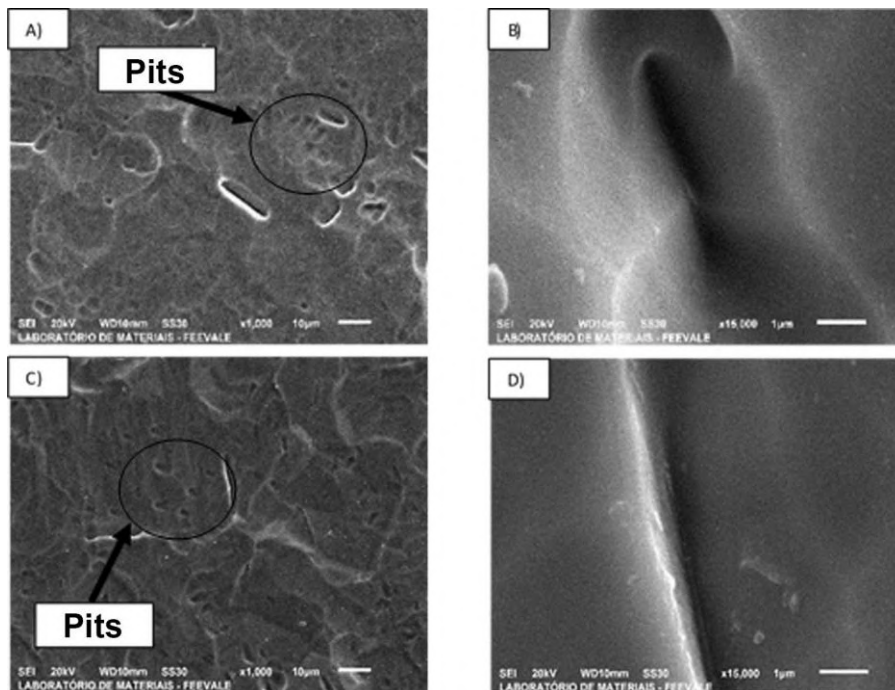
Source: Authors.

In Figure 6, both sets of images (A and C at 1000x magnification and B and D at 15000x magnification) showed great similarity in relation to their morphology for both magnifications, which indicates the repeatability of the process as both samples were anodized under the same conditions. In images A and C at 1000x magnification (Figure 6), it is possible to observe surface irregularities that are similar to that observed on the surface of the non-anodized sample (Figure 5). However, the presence of pits was also observed in the surface of both samples anodized in the electrolyte of *Psidium guajava* extract for

5 minutes at 0.1 mA/cm², indicating the formation of an oxide layer on the surface after the process. The thickness of the oxide formed during anodization can be considered small, since the potential developed during the process was approximately 6V in 5 minutes (Figure 1). Therefore, the film only grows over the existing topography, overlapping it and replicating its characteristics.

Figure 7 shows the top-view SEM micrographs of two samples anodized in the electrolyte of *Psidium guajava* extract for 30 minutes at 0.1 mA/cm² and at 1000x and 15000x magnifications. Just as samples anodized at 0.1 mA/cm² for 5 minutes, samples anodized at the same current density for 30 minutes (Figure 7) showed great similarity in relation to their morphology at both magnifications, indicating the repeatability of the process. The presence of pits was also observed on the surface of both anodized samples, just as observed at 5 minutes. This indicates the formation of an oxide layer on the surface after the process. Then, as the process develops in galvanostatic mode and at low current density, the amorphous-crystalline transition seems to occur in an equilibrium state with slow changes.

Figure 7. Top-view SEM micrographs of titanium samples anodized in *Psidium guajava* extract for 30 minutes at 0.1 mA/cm². Sample 1 A) 1000x magnification and B) 15000x magnification. Sample 2 C) 1000x magnification and D) 15000x magnification.
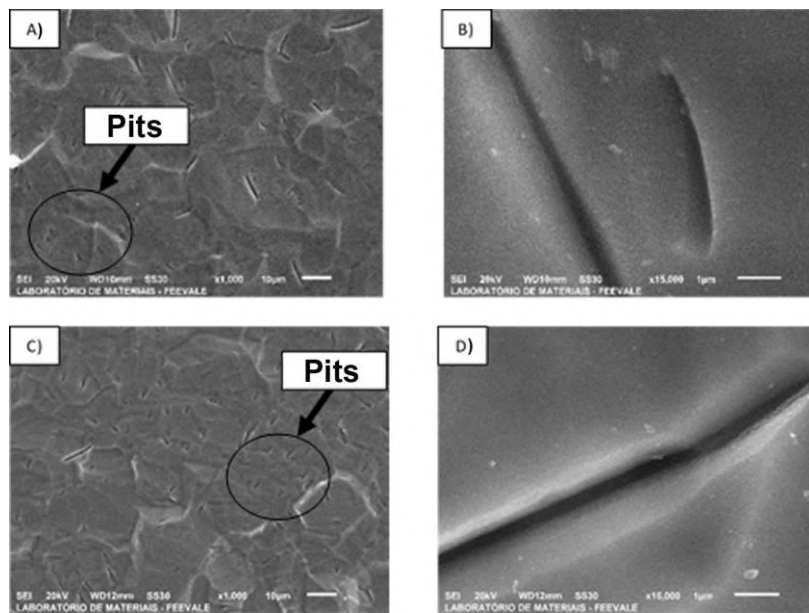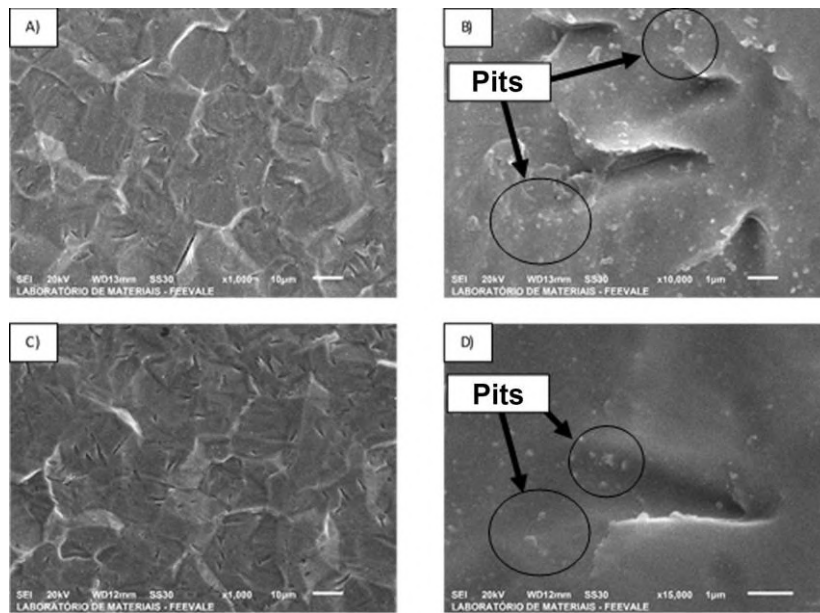

Source: Authors.

Figure 8 shows the top-view SEM micrographs of two samples anodized in the electrolyte of *Psidium guajava* extract for 60 minutes at 0.1 mA/cm² and at 1000x and 15000x magnification.

It is possible to observe in Figure 8 the similarities between images of samples anodized in the electrolyte of *Psidium guajava* extract for 60 minutes at 0.1 mA/cm², which had already been observed at images of 5 and 30 minutes. Additionally, SEM micrographs showed the formation of small agglomerates, such as nodules (Figure 8, images B and D), in the formed oxide film. According to the literature, the oxide initially grows homogeneously up to a limit thickness determined by the applied potential, but agglomerates appear on the oxide surface when it is exposed to a long oxidation time (Raja et al., 2005, Kunst et al., 2021).

Figure 8. Top-view SEM micrograph of titanium samples anodized in *Psidium guajava* extract for 60 minutes at 0.1 mA/cm². Sample 1 A) 1000x magnification and B) 15000x magnification. Sample 2 C) 1000x magnification and D) 15000x magnification.

Source: Authors.

These nodules, also known as "flower-like" structures (Xing et al., 2013; Liu et al., 2014), consist of crystalline oxide nucleus. Its formation is mainly associated with oxygen evolution. Other authors also noted that there is a relationship among potential increase, anodization time, and nodule formation, thus indicating that there was an aging of the film and thickening of the oxide (Fadl-Allah et al., 2010; Vermesse et al., 2013).

3.5 Wettability analysis

The wettability technique was performed on non-anodized (pure) samples and on samples anodized in *Psidium guajava* extract with variation of anodization time (5, 30, and 60 minutes) and current density of 0.1 mA/cm². As in the SEM micrograph analysis, we chose to only analyze samples anodized at 0.1 mA/cm² due to proven reproducibility. Table 4 shows contact angle values obtained by sessile drop technique, which was repeated at 5 different points of the samples.

Table 4. Contact angle values obtained by sessile drop technique.

| Sample	Contact angle (°)	Standard deviation
Pure; not anodized	71	4.2
TI01-5	79	1.5
TI01-5A	77	1.6
TI01-30	80	3.4
TI01-30A	81	1.8
TI01-1H	85	3.1
TI01-1HA	76	5.2

Source: Authors.

The graph represented in Figure 9 provides a better comparison among studied samples.

In Table 4, it is observed that the pure (not anodized) titanium presented a hydrophobic character, with values close to

70 degrees for biomaterials. In the literature, this hydrophobic characteristic is related to the presence of titanium oxide on its surface and small irregularities, which cause a decrease in the surface free energy (Salvador et al., 2017).

Samples anodized for 5 minutes (TI01-5 and TI01-5A) and for 30 minutes (TI01-30 and TI01-30A) had higher contact angle values compared to non-anodized samples (close to 77 and 81 degrees). As discussed for SEM micrographs, the samples showed oxide formation, which is associated with barrier-type oxide with thin thickness, according to the images and the literature. These characteristics only highlights irregularities already existing in the samples. These oxide formations also presented heterogeneous surfaces with small pits in the oxide film (Figure 6 and Figure 7), which may have influenced the less hydrophilic behavior in relation to non-anodized samples.

Figure 9. Graph of the contact angle of analyzed samples.
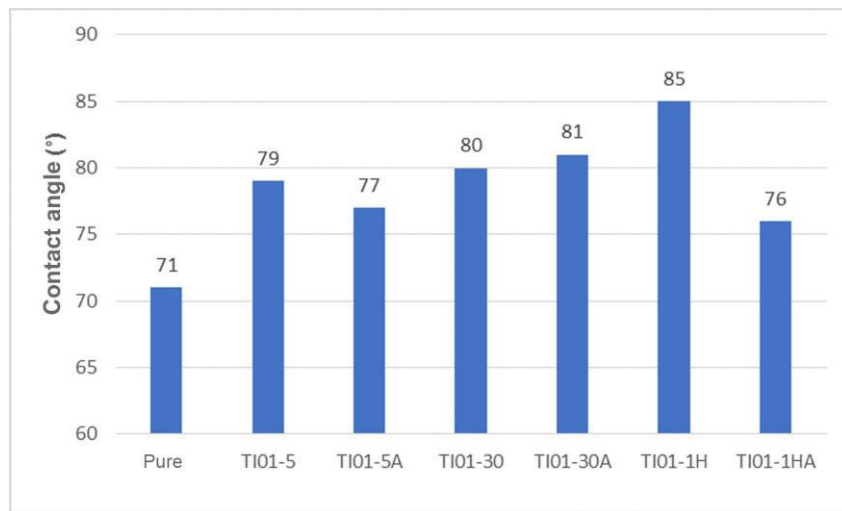
Source: Authors.

The highest values were those obtained for samples anodized for 1 hour (TI01-1H and TI01-1HA). This indicates the formation of a more hydrophobic film, which increases its anticorrosion performance. According to the analysis of SEM micrographs (Figure 8), it was possible to notice that there was an accumulation of oxide material on the surface and the formation of "flower-like" structures, which promote an irregular surface. This information agrees with Table 4, which demonstrated higher standard deviation for these samples. The existence of greater surface irregularity indicates a greater surface area, promoting an increase in the contact area of the coating and causing the corrosion process, which starts on the surface, to happen more quickly (Parra et al., 2006; Filho et al. 2016).

The fact that all samples presented close hydrophobic values for biomaterial parameters confirms the formation of barrier-type oxides. This was also expected due to the fact that there were no significant changes in anodization transients (Figure 1). Additionally, the highest values were obtained for samples that underwent the anodization process for a longer time (1 hour), and consequently had a greater advance in the formation of the oxide film.

The hydrophobicity of the surface is entirely related to the surface energy of the solid and can be evaluated through the contact angle formed by a drop of liquid with the surface. Greater adhesion of liquids results in a smaller contact angle, which indicates a more hydrophilic character in the surface. In this sense, the greater the surface free energy, the greater the wettability and the adhesion of liquids.

In contrast, the degree of hydrophobicity promoted by a surface coating is directly related to its ability to provide anticorrosion protection and is proportional to the contact angle of the liquid with the surface coating. The higher the contact angle, the higher the hydrophobicity of the material and, consequently, the lower the influence of humidity on its eventual

corrosive processes (Gama, 2014; Prodócimo, 2008; Serafim, 2013). Regarding the samples of the present study, it was observed that there is a very small variation over the anodization time, which indicates that the oxide obtained in *Psidium guajava* is quite fine.

3.6 UV-Visible

Figure 10 shows UV-visible spectra of the electrolyte of *Psidium guajava* extract before and after the anodization.

Figure 10. UV-visible absorption spectrum of *Psidium guajava* extract pre- and post-anodization.
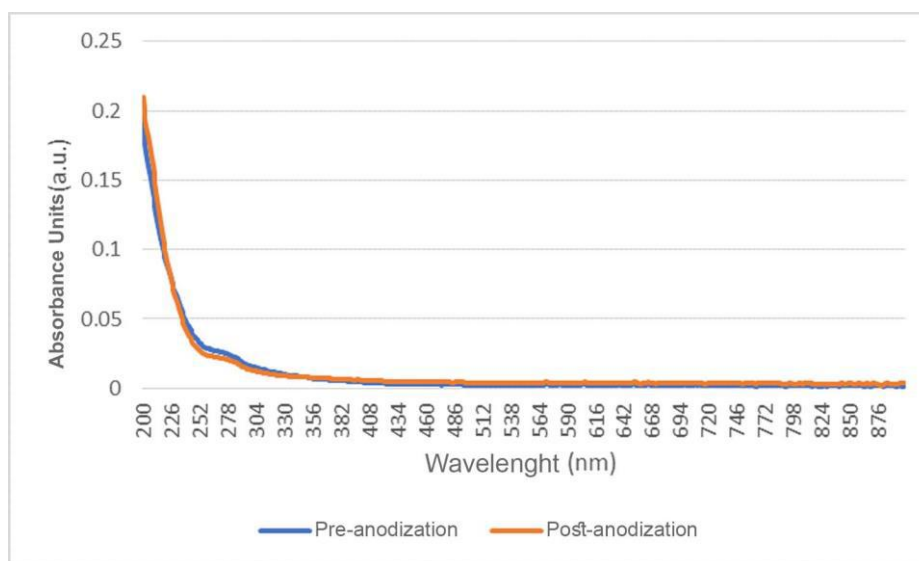
Source: Authors.

In Figure 10, the curves presented a very similar behavior, almost overlapping. The spectrum also showed an absorption peak at a wavelength of approximately 275 nm, which is attributed to the characteristic absorption of phenolic groups according to the literature (Somchaidee et al. 2018).

Studies performed by Somchaidee et al., 2018 have indicated that if the pH of the *Psidium guajava* extract is adjusted to 3 by adding HCl 0.1 M, there is a decrease in the absorption intensity. Increasing the pH from 5 to 10 promotes a shift in the characteristic peak of a phenolic group to a longer wavelength at about 279 nm. It is believed that the deviation of this peak is due to the delocalization of the electrons of the phenoxides. Additionally, it is also believed that most ligands remain protonated at lower pH and deprotonation increases at higher pH. However, the absorption intensity decreases at pH 10. This change may be due to partial precipitation of the extract due to the use of a high ionic strength of the solution. The results suggest that the adjustment of the pH of the guava leaf extract to 8 could provide maximum extension of the deprotonated phenolic groups of the tannins for the formation, reduction, and stabilization of zero valent iron complexes from iron ions.

3.7 Cyclic voltammetry

Cyclic voltammetry is considered an important electrochemical technique used in electroanalytical chemistry, especially for knowing about the electroactivity of compounds (mainly biological molecules), investigating coupled chemical reactions and studying electrode surfaces. Generally, a conventional cell composed of a system of three electrodes (working electrode (WE), reference electrode (RE) and auxiliary electrode (AE)) is used immersed in a solution kept in a stationary condition. The most important electrode is the working electrode, which is where the reaction of interest takes place. It can be composed of different materials, such as carbon, gold, silver, copper, platinum, nickel, palladium, titanium dioxide, among

others. Experimental parameters are controlled by a potentiostat. In the current-potential voltametric profile, the oxidation and reduction process occurring at the working electrode are represented by anodic peak current (Ipa) and cathodic peak current (Ipc). Figure 11 shows the voltametric profiles obtained for the *Psidium guajava* extract in relation to CP titanium grade 2.

Figure 11. Voltametric profiles registered for the *Psidium guajava* extract at pH 5.5.
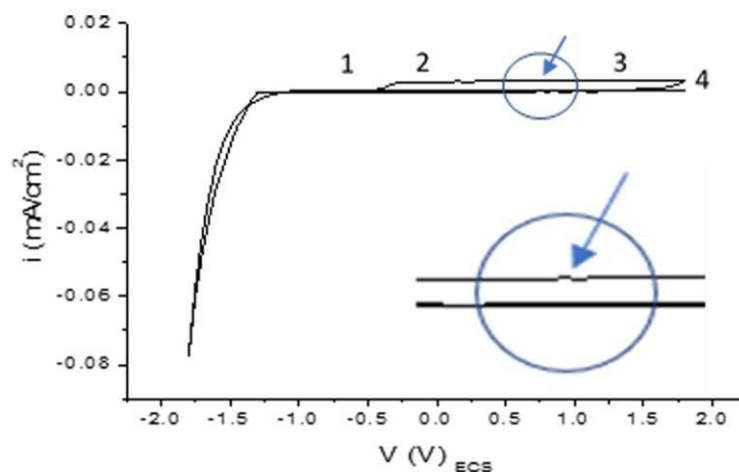
Source: Authors.

Figure 11 shows that the shape of the obtained curves is similar to the typical curves of valve metals found in the literature. These curves are characterized by four main regions, as indicated in Figure 11. Region 1, between the current signal reversal potential and the beginning of the current plateau, is related to the oxidation of the metal to oxide growth in the one that pre-exists in open circuit. Region 2, where the oxide film thickness increases according to the potential, extends to the begging of the oxygen evolution reaction, where Region 3 starts and rises to the threshold potential in which the scanning direction is switched. Lastly, Region 4 is characterized by a sharp decay of the current, tending to zero, in which no current related to oxide reduction is noticed in a wide potential range of the negative-direction potential (Zaniolo et al., 2018).

Furthermore, it is possible to observe in Figure 11 that from -0.5 V, even if not significantly, the release of oxygen begins. According to Ohtsuka et al., 1998, who studied the semiconductor properties of the film grown on pure titanium in 0.1 M sulfuric acid solution and in acid electrolyte, the release of oxygen in quite evident. Despite the pH not being as acid as that of sulfuric acid, the release of oxygen can still be observed in the present study, since the reverse scan (on the turn underneath) indicates that this is not a dissolution process. In addition, the abrupt drop in current (on the loop) indicates an important capacitive current and/or a high film resistance.

The voltammogram of the Figure 11 also shows a slight peak (indicated in the figure) at approximately 1 V. A similar behavior was also observed by Ouafy et al., 2014, who attributed this peak to the presence of phenolics in the electrolyte. This result corroborates the results obtained in the UV-Vis (Figure 10), which evidenced the presence of phenolic compounds in the electrolyte. In the study performed by Ouafy et al., 2014, a well-defined oxidation peak was observed at approximately 1 V for a phenol concentration of 0.004 M. This indicates that the concentration of phenolics in the electrolyte of the present study is lower than that of Ouafy et al., 2014, which may be due to the dilution performed in the preparation of the extract.

Only one anodic oxidation peak was observed, suggesting that the electrochemical process of phenol is irreversible. Ouafy et al., 2014 also found that the anodic peak current increases linearly with the phenol concentration, indicating that the electrode process is an adsorption-controlled reaction. The study performed by Ouafy et al., 2014 indicated that the higher the

concentration, the greater the identification of the peak of phenolics at potentials starting from 1 V, and that lower concentrations present potentials between 0.8 and 0.9 V, which was also observed in the present study.

4. Conclusion

All anodizations performed on titanium and using an electrolyte based on *Psidium guajava* extract at current density transients of 0.1 and 1 mA/cm² for 5, 30 and 60 minutes, showed the formation of an oxide layer. However, the non-reproducibility in tests performed at the current density of 1 mA/cm² was evident in the anodization graphs.

It was also observed that samples showed similar colors in tests performed at 0.1 mA/cm² at different anodizing times, but very different colors in tests performed at 1 mA/cm². It is assumed that the rapid consumption of electrolyte species at 1 mA/cm² is associated with non-reproducibility.

Regarding the results of different anodizing times at 0.1 mA/cm², it was observed that samples showed similar results at 5 and 30 minutes, indicating reproducibility. In addition, irregularities on the surface were similar to that on the surface of the non-anodized sample. In samples anodized at 0.1 mA/cm² for 60 minutes, the formation of small agglomerates, known as "flower-like" structures, was observed in SEM micrographs. Thus, indicating that there was an aging of the film and thickening of the oxide.

As for hydrophobicity results, all samples presented relatively close hydrophobic values for biomaterial parameters, confirming the formation of barrier-type oxides.

Analyses of the electrolyte of *Psidium guajava* suggest the possible presence of phenolic groups in the electrolyte composition. UV-Vis spectra showed similar behavior curves before and after the anodizing process, and cyclic voltammetry results agree with those presented in the UV-Vis, since that there was only one anodic oxidation peak. This may be associated to the presence of phenolic compounds in the electrolyte, suggesting that the electrochemical process of phenol is completely irreversible.

Therefore, it can be concluded that samples presenting the best results in relation to the formation of oxide layer and reproducibility were those anodized in *Psidium guajava* extract for 5 and 30 minutes, at current density of 0.1 mA/cm². The results suggest that the formation of an oxide layer may be associated with the presence and concentration of phenolic compounds in the electrolyte.

Acknowledgements

References

Alves, A. K. (2008). Obtenção de micro e nanofibras de TiO_2 por eletrospinning: caracterização de propriedades e atividade fotocatalítica. *Tese (Doutorado) - Escola de Engenharia. Programa de Pós-Graduação em Engenharia Minas, Metalúrgica e de Materiais, Universidade Federal do Rio Grande do Sul.* Porto Alegre, 136f.

Amorim, A., Comunian, C. R., Neto, M. D. F., & Cruz, E. F. (2019). Implantodontia: Histórico, evolução e atualidades/Implantology: History, Evolution and News. *Revista de psicologia*, 13(45), p. 36-48.

Catauro, M., Bollino, F., Papale, F., Giovanardi, R., & Veronesi, P. (2014). Corrosion behavior and mechanical properties of bioactive sol-gel coatings on titanium implants. *Materials Science and Engineering: C*, 43, p. 375-382.

Chen, J., Wang, J., & Yuan, H. (2013). Morphology and performances of the anodic oxide films on Ti6Al4V alloy formed in alkaline-silicate electrolyte with aminopropyl silane addition under low potential, *Applied Surface Science*, 284, p. 900–906.

Fadl-Allah, S. A., & Mohsen, Q. (2010). Characterization of native and anodic oxide films formed on commercial pure titanium using electrochemical properties and morphology techniques. *Applied Surface Science*, 256(20), p. 5849-5855.

Fernandes, M., Kunst, S. R., Morisso, F. D. P., Carús, L.A., Ziulkoski, A. L., & Oliveira, C. T. (2022). Inserção de nanocargas de prata em superfície de titânio anodizado. *Research, Society and Development*, 11, p. e13711729690.

Fuhr, L. T., Moura, A. B. D., Carone, C. L. P., Morisso, F. D. P., Scheffel, L. F., Kunst, S. R., Ferreira, J. Z., & Oliveira, C. T. (2020). Colored anodizing of titanium with pyroligneous solutions of black wattle. *Matéria (Rio de Janeiro)*, 25(2), p. 12658.

Galan, J. R., Viera, J., & Namen R. M. (2013). Caracterização das superfícies de implantes dentais comerciais em MEV/ED. *Revista Brasileira de Odontologia*, 70(1), p. 68.

Gama, R. O. (2014). Controle do comportamento hidrofílico/hidrofóbico de polímeros naturais biodegradáveis através da decoração de superfícies com nano e microcomponentes. *Tese (Doutorado) - Curso de Engenharia Metalúrgica, Materiais e de Minas, Universidade Federal de Minas Gerais*, Belo Horizonte, 110 f.

Hsueh, Y. H., Cheng, C. Y., Chien, H. W, Huang, X. H, Huang, C. W., Wu, C. H., Chen, S. T., & Ou, S. F. (2020). Synergistic effects of collagen and silver on the deposition characteristics, antibacterial ability, and cytocompatibility of a collagen/silver coating on titanium. *Journal of Alloys and Compounds*, 830, p. 15-25.

Indira, K., Mudali, U. K., Nishimura, T., & Rajendran, N. (2015). A Review on TiO_2 Nanotubes: influence of anodization parameters, formation mechanism, properties, corrosion behavior, and biomedical applications. *Journal of Bio-and Tribo-Corrosion*, 1(4), p. 127-134.

Kociubczyk, A. I., Vera, M. L., Schvezov, C. E., Heredia, E., & Ares, A. E. (2015). TiO_2 coatings in alkaline electrolytes using anodic oxidation technique. *Procedia Materials Science*, 8, p. 65-72.

Kunst, S. R., Cerveira, D. O., Ferreira, J. Z., Graef, T. F., Santana, J. A., Carone, C. L. P., Morisso, F. D. P., & Oliveira, C. T. (2021). Influence of simulated body fluid (normal and inflammatory) on corrosion resistance of anodized titanium. *Research, society and development*, 10, p. e122101018606.

Kuromoto, N. K., Simão, R. A., & Soares, G. A. (2007). Titanium oxide films produced on commercially pure titanium by anodic oxidation with different voltages. *Materials Characterization*, 58(2), p. 114-121.

Lee, W., Scholz, R., & Gösele, U. A. (2008). Continuous process for structurally well-defined Al_2O_3 nanotubes based on pulse anodization of aluminum. *Nanoletters*, 8(8), p. 2155-2160.

Liu, Z., Liu, H., Zhong, X., Hashimoto, T., Thompson, G. E., & Skeldon, P. (2014). Characterization of anodic oxide growth on commercially pure titanium in NaTESi electrolyte. *Surface and Coatings Technology*, 258, p. 1025-1031.

Marcus, P., & Maurice, V. (2000). Passivity of metals and alloys. *Material Science and Technology*. Wiley-VCH Verlag GmbH & Co KGaA.

Mueller, L. P., Fleck, J. D., Fuhr, L. T., Caroni, C. L. P., & Kunst, S. R. (2019). Emprego de extrato de *Psiduum guajava* como eletrólito e processo de obtenção. *Patente BR 10 2019 027581 2* em 20 de dezembro de 2019.

Nakajima, M., Miura, Y., Fushimi, k., & Habazaki, H. (2009). Spark anodizing behaviour of titanium and its alloys in alkaline aluminate electrolyte. *Corrosion Science,* 51(7), p. 1534-1539.

Naseer, S., Hussain, S., Naeem, N., et al. (2018). The phytochemistry and medicinal value of *Psidium guajava* (guava). *Clinical Phytoscience,* 4(32), p. 1.

Ohtsuka, T., & Otsuki, T. (1998). The influence of the growth rate on the semiconductive properties of titanium anodic oxide films. Corrosion Science, 40(6), p. 951-958.

Ory, F., Fraysse, J. L. (2018). Titanium and titanium alloys: Materials, review of processes for orthopedics and a focus on a proprietary approach to producing cannulated bars for screws and nails for trauma. *Titanium in Medical and Dental Applications*. 65-91, p. 303-324.

Ouafy, T., Chtaini A., Oulfajrite, H., & Najih R. (2014). Electrochemical determination of phenol at natural phosphate modified carbon paste electrode. *Leonardo Electronic Journal of Practices and Technologies*, 25, p. 166-178.

Parra, B. S., Gennari, R. C., Melchiades, F. G., & Boschi, A. O. (2006). Rugosidade superficial de revestimentos cerâmicos. *Cerâmica industrial*, 11(2), p.15-18.

Prodócimo, K. E. (2008). Estudo da modificação superficial por ataque químico em chapas de aço inoxidável AISI 430, visando à adesão de revestimentos poliméricos. *Trabalho de Conclusão de Curso - Graduação em Engenharia de Materiais* - Universidade Federal de Santa Catarina, Florianópolis.

Quintero, D., Galvis, O., Calderón, J. A., et al. (2014). Effect of electrochemical parameters on the formation of anodic films on commercially pure titanium by plasma electrolytic oxidation ‖. *Surface and Coatings Technology*, 258, p. 1223-1231.

Rahman, Z. U., Haider, W., Pompa, L., & Deen, K. M. (2016). Electrochemical & osteoblast adhesion study of engineered TiO_2 nanotubular surfaces on titanium alloys. Materials Science and Engineering: C, 58, p. 160-168.

Raja, K. S., Misra, M., & Paramguru, K. (2005). Formation of self-ordered nano-tubular structure of anodic oxide layer on titanium. *Electrochimica Acta*, 51, p. 154–165.

Ribeiro Filho, S. L. M., Lauro, C. H., Bueno, A. H. S., et al. (2016). Influence cutting parameters on the surface quality and corrosion behavior of Ti-6Al-4V alloy in synthetic body environment (SBF) using Response Surface Method. *Measurement*, 88, p. 223–237.

Salvador, D. G., Marcolin, P., Beltrami, L. V. R., Brandalise, R. N., & Kunst, S. R. (2017). Influence of the pretreatment and curing of alkoxysilanes on the protection of the titanium-aluminum-vanadium alloy. *Journal of Applied Polymer Science*, 134(46), p. 45470.

Saurabh, A., Meghana, C. M., Singh, P. K., & Verma, P. C. (2022). Titanium-based materials: synthesis, properties, and applications. *Materials Today: Proceedings,* 56 (1), p. 412-419.

Serafim, J. (2013). Avaliação do Pré Tratamento a base de sulfossiloxano sobre aço galvannealed combinado com tintas anticorrosivas. *Dissertação de Mestrado - Escola Politécnica da Universidade de São Paulo*, São Paulo, 106 f.

Somchaidee, P., & Tedsree, k. (2018). Green synthesis of high dispersion and narrow size distribution of zero-valent iron nanoparticles using guava leaf (*Psidium guajava* L) extract. *Advances in Natural Sciences: Nanoscience and Nanotechnology*, 9, p. 035006.

Sul, Y. (2001). The electrochemical oxide growth behavior on titanium in acid and alkaline electrolytes. *Medical Engineering and Physics*, 23(1), p.329-346.

Umoren, S., Solomon, M., Obot, I., & Sulieman, R. (2019). A critical review on the recent studies on plant biomaterials as corrosion inhibitors for industrial metals. *Journal of Industrial and Engineering Chemistry*, 76(25), p. 91-115.

Vermesse, E., Mabru, C., & Arurault, L. (2013). Applied Surface Science Surface integrity after pickling and anodization of Ti – 6Al – 4V titanium alloy. *Applied Surface Science*, 285, p. 629–637.

Verma, R. P. (2020). Titanium based biomaterial for bone implants: a mini review. *Materials Today: Proceedings*, 26, p. 3148-3151.

Xing, J., Xia, Z., Hu, J., Zhang, Y., & Zhong, L. (2013). Time dependence of growth and crystallization of anodic titanium oxide films in potentiostatic mode. *Corrosion Science*, 75, p. 212–219.

Young, L., Dell'oca, C. J., & Pulfrey, D. L. (1971). Anodic oxide films. *Physics of thin films*. Elsevier, p. 1-79.

Zaniolo, K. M., Biaggio, S. R., Bocchi, N., & Rocha-Filho, R. C. (2018). Properties of colored oxide films formed electrochemically on titanium in green electrolytes under ultrasonic stirring. *Journal of Materials Science*, 53(10), p. 7294-7304.

Zaniolo, K. M. (2015). Crescimento Anódico e caracterização de óxidos de titânio em eletrólitos alternativos. *Dissertação (Mestrado em Química) – Programa de Pós-Graduação em Química. Universidade Federal de São Carlos -UFSCar)*, São Carlos, 136 f.